Journal of Materials Chemistry B

RSC Publishing

PAPER

View Article Online
View Journal | View Issue

Cite this: *J. Mater. Chem. B*, 2013, **1**, 1296

Structural characterisation of hypoxia-mimicking bioactive glasses†

Jodie M. Smith,[a] Richard A. Martin,*[b] Gabriel J. Cuello[c] and Robert J. Newport[a]

Received 13th November 2012
Accepted 10th January 2013

DOI: 10.1039/c3tb00408b

www.rsc.org/MaterialsB

Nickel and cobalt are both known to stimulate the hypoxia-inducible factor-1 (HIF-1α), thus significantly improving blood vessel formation in tissue engineering applications. We have manufactured nickel and cobalt doped bioactive glasses to act as a controlled delivery mechanism of these ions. The resultant structural consequences have been investigated using the methods of isotopic and isomorphic substitution applied to neutron diffraction. The structural sites present will be intimately related to their release properties in physiological fluids such as plasma and saliva, and hence the bioactivity of the material. Detailed structural knowledge is therefore a prerequisite for optimising material design. Results show that nickel and cobalt adopt a mixed structural role within these bioactive glasses occupying both network-forming (tetrahedral) and network-modifying (5-fold) geometries. Two thirds of the Ni (or Co) occupies a five-fold geometry with the remaining third in a tetrahedral environment. A direct comparison of the primary structural correlations (*e.g.* Si–O, Ca–O, Na–O and O–Si–O) between the archetypal 45S5 Bioglass® and the Ni and Co glasses studied here reveal no significant differences. This indicates that the addition of Ni (or Co) will have no adverse effects on the existing structure, and thus on *in vitro*/*in vivo* dissolution rates and therefore bioactivity of these glasses.

1 Introduction

Vascularisation is essential in wound healing for both soft and hard tissue regeneration. Bio-oxygen levels play an important role in modulating cell functions and tissue repair *in vivo*. Hypoxia (low oxygen partial pressure) can enhance the production of specific extracellular matrix components and increase blood vessel formation (angiogenesis) through the hypoxia-inducible factor-1 (HIF-1α) pathway.[1] For example, HIF-1α over-expressing bone marrow stem cells significantly improve blood vessel formation in bone tissue engineering applications.[2] Wan *et al.* demonstrated that the HIF-1α pathway is activated during bone repair and can be manipulated to improve skeletal healing.[3] Reduced oxygen levels have also been shown to stimulate chondrogenesis in stem cells, which is important for cartilage regeneration.[4]

Transition metals such as Co and Ni have been shown to increase the HIF-1α transcription factor.[5] Bioactive glasses offer an exciting route for potential delivery systems of transition metal ions within tissue regeneration scaffolds due to their ability to incorporate a large variety of elements and their largely controllable dissolution properties within physiological fluids.[6] Bioglass®, developed by Hench, was developed to provide a controlled release of calcium and phosphorous ions under physiological conditions.[7] These ions then precipitate into amorphous calcium phosphate which later crystallise into hydroxyapatite to form new bone mineral.[8–10] In addition to providing the fundamental building blocks of bone (Ca and P) the dissolution products of bioglass were also found to stimulate osteoblast activity.[11,12] More recently bioactive glasses have been developed to provide a controlled release mechanism for antimicrobial ions such as Ag and Ga to combat infections.[13,14]

In order to be able to model and predict the behaviour of bioactive glasses *in situ* it is important to have an understanding of the atomic scale structure and any modifications that may result due to the incorporation of additional elements. However, the structure of bioglass is particularly complex owing to the addition of two network modifiers (Na and Ca) into a glass composed of two network formers (Si and P). Significant progress has now been made on unravelling the atomic scale structure of archetypal 45S5 Bioglass through a series of molecular dynamic simulations,[15–17] nuclear magnetic resonance[18–20] and neutron diffraction studies.[21–24] CaO and Na_2O both adopt network modifier roles, breaking Si–O–Si bonds through the addition of oxygen. Other elements such as Zn, Mg, Ga and Al have been found to act as network intermediates where they can act as network formers, network modifiers or a mixture of both network formers and modifiers.[25,26]

[a]*School of Physical Sciences, University of Kent, Ingram Building, Canterbury, CT2 7NH, UK*

[b]*School of Engineering & Applied Science and Aston Research Centre for Healthy Ageing, University of Aston, Aston Triangle, Birmingham, B4 7ET, UK. E-mail: R.A. Martin@Aston.ac.uk*

[c]*Institut Laue-Langevin, BP 156, F-38042, Grenoble Cédex 9, France*

† Electronic supplementary information (ESI) available. See DOI: 10.1039/c3tb00408b

The addition of a transition metal further complicates the picture as it is not possible to predict *a priori* the structural consequences of their incorporation into bioactive glasses. Cobalt, for example, could adopt various structural arrangements, as discussed by Azevedo *et al.*, including entering the silicate network as four-fold Co–O or acting as a network modifier with a resultant higher coordination number up to possibly eight-fold Co–O.[27] The role of cobalt (or Ni) in the glass network will determine the network connectivity (NC) and macroscopic properties, such as ion release rates and hydroxyapatite formation. Cobalt and nickel both have similar ionic radii and charge states that also closely match magnesium. According to Shannon, the ionic radii of four-fold Ni, Co and Mg are 0.58, 0.55 and 0.57 Å respectively.[28] Given the similar ionic radii and therefore similar charge to size ratio it may be expected that Co and Ni will adopt a similar structural role to that of Mg, which has been shown to act as a network intermediate.[25] Furthermore, Na^+ and Ca^{2+} ions both show an affinity for phosphate species over silicates;[29] again, it is difficult to predict the most energetically favourable environment of transition metals and their preferred structure.

Ultimately, the resultant structural influence of the transition metals may determine which applications these glasses are most suitable for (*e.g.* soft or hard tissue regeneration). For example, replacing Ca with Sr within the glass leads to an expanded matrix which results in an increased solubility and an increased rate of hydroxyapatite formation, which is highly desirable for bone regeneration applications.[30] Conversely, replacing Ca with Mg within the glass leads to a contracted matrix and decreased rate of HA formation.[25] For soft tissue applications such as cartilage regeneration a reduction in HA formation is desirable. Importantly, the local environment surrounding the transition metal will strongly influence its rate of dissolution from the glass. A fast release of transition metals will result in a high local concentration, which is known to cause cell toxicity.[31] A controlled release rate, appropriate to enhanced angiogenesis, is therefore vital for any tissue engineering application.

It is important that detailed experimental studies are conducted to elucidate the structural consequences of incorporating transition metals into bioactive glasses. We report here on a detailed investigation of the structural effects of incorporating Ni and Co into bioactive glasses using advanced neutron diffraction techniques. 4 mol% NiO (or Co) was incorporated into bioglass to provide physiologically appropriate concentrations.[27,32] Cobalt is cytotoxic in high concentrations however Wu *et al.* have shown that bioactive scaffolds containing less than 5 mol% CoO are not cytotoxic.[32] The low concentration of transition metals incorporated in these glasses means it is not possible to extract structural information from a single total (*i.e.* conventional) diffraction pattern. By employing the method of isotopic substitution applied to neutron diffraction we have isolated the nickel correlations, providing definitive quantitative structural information on the local environment surrounding the nickel ions. In addition, by applying the method of isomorphic substitution between Co and Ni bioactive glasses, we have been able to confirm that Co adopts the same structural environment within these glasses.

2 Experimental

Sample preparation

Melt-quenched glass samples were prepared using SiO_2 (Alfa Aesar, 99.5%), $CaCO_3$ (Alfa Aesar, 99.95–100.5%) and Na_2CO_3 (Sigma-Aldrich, 99.5+%), $NH_4H_2PO_4$ (Sigma-Aldrich, ≥99.5%), and the selected transition metal. The isotopically enriched Ni doped bioactive glasses were prepared using metallic 99.5% enriched ^{58}Ni, ^{nat}Ni and 98% enriched ^{62}Ni (ISOFLEX) respectively. Metallic Ni oxidises during the heating process to form nickel(II) oxide; a control sample was also prepared using ^{nat}NiO and no difference in the XANES spectra or density measurements could be observed between samples prepared using metallic or oxide nickel. Cobalt doped bioactive glasses were prepared CoO (Alfa Aesar, 99.995%). The ratio of precursors was selected to yield glasses with compositions of Bioglass® 45S5 + 4 mol% transition metal oxide. The precursors, after thorough mixing, were heated in a platinum–rhodium (10%) crucible at a rate of 10 °C min^{-1} to 1450 °C and held at this temperature for 90 minutes. The melt was poured into a graphite mould which had been preheated to 450 °C and annealed at this temperature overnight before being allowed to cool slowly to room temperature. The resultant glass compositions were $(MO)_{3.8}(SiO_2)_{44.3}(CaO)_{25.9}(Na_2O)_{23.5}(P_2O_5)_{2.5}$, where M represents the transition metal Ni or Co.

Density measurements

Density measurements were taken using a Quantachrome pycnometer using Archemedes' method with helium being used as the fluid.

Ni and Co K-Edge XANES/EXAFS

Measurements were undertaken on the B18 instrument at the Diamond Light Source, Harwell Research Campus. Finely ground samples were diluted in cellulose and pressed into pellets to give a satisfactory K-edge absorption step. The spectra were recorded at room temperature and in transmission mode. The incident beam intensity and the transmitted beam intensity were measured using ionization chambers. The Ifeffit software analysis suite was used for the background corrections and normalisation (Athena).[33] The data analysis was undertaken using pyspline.[34] In brief, the data processing comprised calibrating the energy scale, normalizing the incident beam intensity and the spectra to provide an edge step of one. The data modelling was undertaken using EXCURV.[35]

Neutron diffraction

The neutron data was collected at the D4 diffraction instrument at the Institut Laue-Langvin, Grenoble.[36] Calibration of the incident neutron wavelength was achieved using a polycrystalline nickel reference sample. The samples were ground into course lumps and contained in vanadium cans of internal diameter 6 mm and wall thickness 0.25 mm; a vanadium rod of diameter 6 mm was used to provide quantitative normalisation to the data. Data were collected from the empty instrument, empty vanadium container and the vanadium rod in addition to

each of the samples. Structural information can be obtained from the data by removing the background scattering (from the instrument itself and from the container) and correcting for absorption and multiple scattering to find the differential cross-section using the program CORRECT.[37,38]

The total structure factor is given by[39]

$$i(Q) = \sum_i \sum_j c_i c_j b_i b_j [\rho_{ij}(Q) - 1] \quad (1)$$

where c_i and b_i denote the atomic fraction and coherent scattering length of the chemical species i, $\rho_{ij}(Q)$ is the partial structure factor and Q is the magnitude of the scattering vector given by $Q = 4\pi\sin(\theta)/\lambda$ where 2θ is the scattering angle and λ is the incident neutron wavelength. These functions of Q are referred to as reciprocal space data. The corresponding real-space data is obtained by Fourier transforming the total structure factor to give $T(r)$, where

$$T(r) = T^0(r) + \frac{2}{\pi}\int_0^\infty Qi(Q)M(Q)\sin(Qr)\mathrm{d}Q \quad (2)$$

$M(Q)$ is the window function that takes into account the finite experimentally obtainable maximum value of Q, in this case the quality of the data was sufficient to permit the use of a step function. $T^0(r)$ is the average density term, given by:[39]

$$T^0(r) = 4\pi r\rho^0(\sum_i c_i b_i)^2 \quad (3)$$

where ρ^0 is the macroscopic number density. The pair distribution function that results from a neutron diffraction experiment, $T(r)$, can be represented as the weighted sum of partial correlation functions, $t_{ij}(r)$.

$$T(r) = \sum_{i,j} c_i c_j b_i b_j t_{ij}(r) \quad (4)$$

Examining eqn (4), it can be seen that, if samples are prepared that are identical except for the scattering length of one element, differences between the neutron scattering data from these samples will isolate the partial correlation functions. Since different isotopes (or isomorphs) of an element, have different neutron scattering lengths, isotopic (or isomorphic) substitution provides a method for achieving this separation. In the work presented here the scattering length of the nickel isotope was varied between a set of otherwise identical samples allowing isotopic substitution. Nickel was exchanged for cobalt to allow the isomorphic substitution. The difference in real space can be represented in terms of the partial pair correlation function, $T_{M-j}(r)$, such that only the environment of element M is probed.

$$T_{M-j}(r) = T(r) - T'(r) = c_M{}^2(b_M{}^2 - b'_M{}^2)t'_{MM}(r) + 2\sum_{j\neq M} c_M c_j b_j (b_M - b'_A)t'_{Mj}(r) \quad (5)$$

Structural information can be obtained by modelling the real-space correlation function. Pair functions, $p_{ij}(Q)$, are generated in Q-space and Fourier transformed to allow comparison with the experimental data in real space. The pair functions are given by:[13,40]

$$p_{ij}(Q) = \frac{N_{ij}w_{ij}}{c_j}\frac{\sin(Qr_{ij})}{Qr_{ij}}\exp\left[\frac{-Q^2\sigma_{ij}{}^2}{2}\right] \quad (6)$$

where N_{ij}, r_{ij}, and σ_{ij} are the coordination number, atomic separation and disorder parameter (*i.e.*, a measure of static and thermal disorder) respectively of atom i in relation to atom j. The weighting factors w_{ij} for a standard neutron diffraction experiment are given by:

$$w_{i\neq j} = 2c_i c_j b_i b_j \quad (7)$$

$$w_{i=j} = c_i{}^2 b_i{}^2 \quad (8)$$

In the case of the isomorphic and isotopic difference the weighting factors take the form:

$$w_{i\neq j} = 2c_i c_j (b_M - b'_M)b_j \quad (9)$$

$$w_{i=j} = c_i{}^2(b_M{}^2 - b'_M{}^2) \quad (10)$$

In this case atom M is the transition metal, either nickel or cobalt. Nickel has several naturally occurring stable isotopes: ^{58}Ni has a neutron scattering length, b, of 14.4 fm, whereas ^{62}Ni has $b = -8.7$ fm, ^{nat}Ni has $b = 10.3$ fm and Co has $b = 2.49$ fm.[41]

3 Results and discussion

Bioactive glasses containing 3.8 mol% NiO or CoO were prepared. Three Ni samples were prepared: one containing natural abundance Ni, a second containing nickel enriched with ^{58}Ni and a third enriched with ^{62}Ni. The coherent scattering lengths of the nickel within the ^{58}Ni-, ^{nat}Ni- and ^{62}Ni-enriched glasses, allowing for the levels of isotopic enrichment, are 14.3, 10.3 and −8.4 fm respectively. The negative scattering lengths arise from a π phase shift of the neutron wave function on scattering. Glass samples are hereafter labelled ^{nat}Ni, ^{58}Ni and ^{62}Ni respectively. The densities of all the Ni and Co doped glasses were 2.83(1) g cm^{-3} with a corresponding number density of 0.0769(2) atoms per cubic Angström. Extended X-ray Absorption Fine Structure (EXAFS) data showed no differences between the local Ni–O environments for each of the Ni doped glasses (see ESI, Fig. S1†), thus further confirming that all of the samples were iso-structural.

Neutron diffraction with isotopic substitution

The total interference functions, $i(Q)$, for ^{58}Ni, ^{nat}Ni and ^{62}Ni are shown in Fig. 1. The real space data obtained by Fourier transforming the total interference functions is given in Fig. 2. It is apparent that the real-space datasets are qualitative similar *e.g.* the P–O and Si–O peaks at ~1.6 Å and the Na–O, Ca–O and O–(P)–O, O–(Si)–O peaks around 2.3 to 2.7 Å. The main difference visible in the total diffraction patterns, $T(r)$, occurs in the region around 2 Å where the Ni–O correlation is predicted to occur.[42,43] However, the relatively small weighting factor of the Ni–O correlation (due to the low atomic concentration present) coupled with the overlapping correlation functions makes it difficult unambiguously to fit the Ni–O correlation solely from

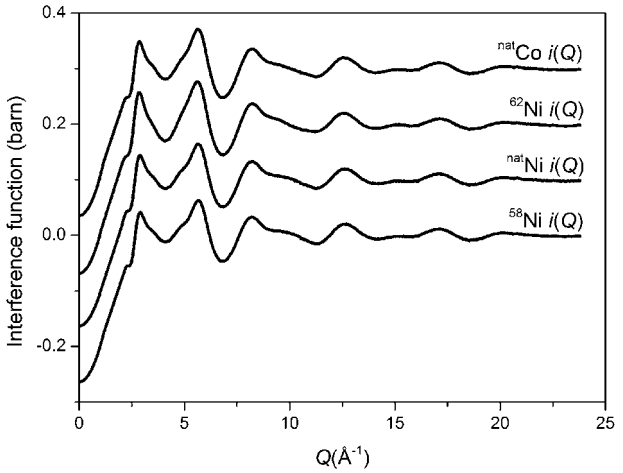

Fig. 1 Total interference functions for the Ni and Co doped bioactive glasses.

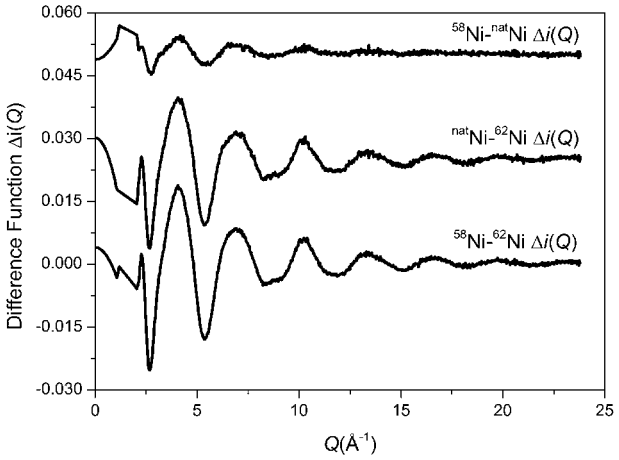

Fig. 3 First order difference isotopic substitution functions $\Delta i(Q)$.

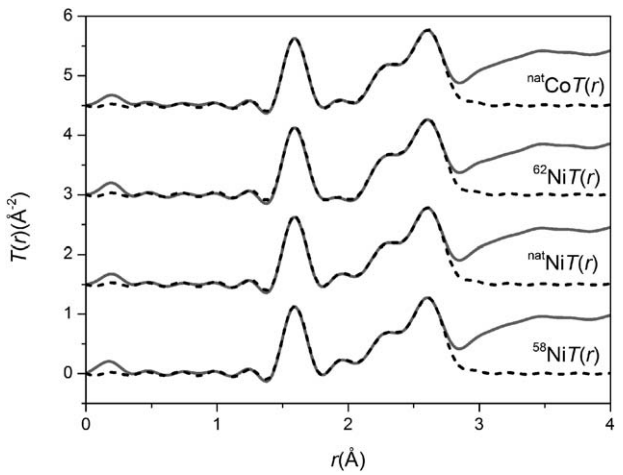

Fig. 2 Real space data for the total diffraction patterns. The solid curve represents the experimental data and the broken curve represents the resultant fits.

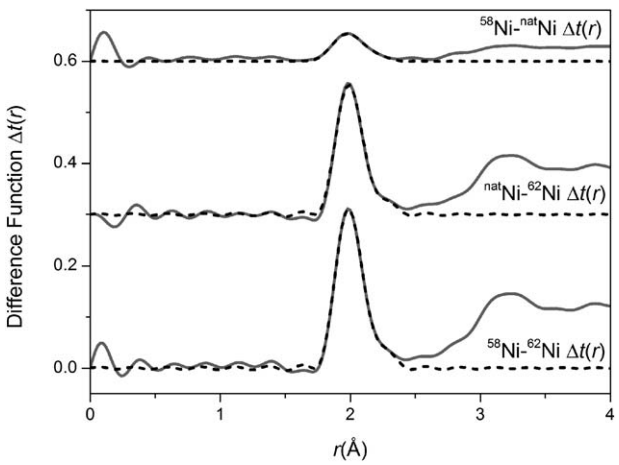

Fig. 4 Real space data for the isotopic substitution difference functions. The solid curve represents the experimental data and the broken curve represents the resultant fits.

the total diffraction pattern. Those correlations not involving Ni can be eliminated by subtracting two total structure factors to give a first order difference function such as $\Delta i(Q)^{58-62} = i(Q)^{58}\mathrm{Ni} - i(Q)^{62}\mathrm{Ni}$ (see Table S1 of the ESI†). The addition of the third total structure factor enables three separate first order difference functions to be determined ($\Delta i(Q)^{58-62}$, $\Delta i(Q)^{58-\mathrm{nat}}$ and $\Delta i(Q)^{\mathrm{nat}-62}$) in order to check the reliability/mutual consistency of the derived datasets. Fig. 3 presents the three isotopic substitution difference functions in reciprocal space, whilst Fig. 4 shows the real space pairwise correlation data $\Delta T(r)$ obtained by Fourier transforming the $\Delta i(Q)$ functions given in Fig. 3. Those correlations not containing Ni successfully cancel, as demonstrated by the absence of the P–O and Si–O peaks at ~1.6 Å. The main feature at ~2 Å correspond to nearest neighbour Ni–O correlations. The broad feature at $\sim 3 < r$ (Å) < 3.5 corresponds to next nearest neighbours correlations such as Ni–(O)–Si, Ni–(O)–P, Ni–(O)–Na and Ni–(O)–Ca; it is not possible unambiguously to resolve these overlapping correlations. As shown in Fig. 4, $\Delta T(r)^{58-62}$ has the largest difference in Ni scattering lengths (22.7 fm) and correspondingly results in best signal-to-noise ratio, $\Delta T(r)^{\mathrm{nat}-62}$ has a difference in scattering length of 18.7 fm whilst $\Delta T(r)^{58-\mathrm{nat}}$ is the least well defined with a scattering length difference of only 4.0 fm. The diffraction data was modelled using the NXFit program developed by Moss[40] and the NDIS-derived fit parameters obtained for each of the first order difference functions are given in Table 1 together with the average values obtained by calculating an average of the $\Delta T(r)$ functions, weighted by scattering length difference.

As shown, the average number of oxygen atoms around a given Ni atom is 4.67 ± 0.05. This is attributed to ~33% of Ni occupying a 4-fold geometry with the remaining ~67% occupying a 5-fold environment. The correlation around 2 Å is attributed partially to the 4-fold Ni–O and partially to 5-fold Ni–O where there are 4 short bonds (1.98 Å) and one longer bond at 2.19 Å. This places a lower limit of 33% of Ni occupying a tetrahedral (network forming) 4-fold geometry. If a small amount of Ni resides in a higher coordination geometry (*i.e.* octahedral) the fraction of tetrahedral Ni will increase

Table 1 First order difference fit parameters. Typical uncertainties for the distance, coordination number and width parameters are 0.02 Å, 0.05 and 0.05 Å respectively. Note that the error bars associated with the ^{58}Ni–^{nat}Ni correlation are significantly larger due to the lower signal to noise ratio as discussed in the text

	Correlation	r (Å)	N	σ (Å)
^{58}Ni–^{62}Ni	Ni–O	1.98	3.85	0.09
	Ni–O	2.19	0.81	0.10
^{nat}Ni–^{62}Ni	Ni–O	1.99	3.87	0.09
	Ni–O	2.20	0.68	0.10
^{58}Ni–^{nat}Ni	Ni–O	1.96	4.00	0.10
	Ni–O	2.15	1.27	0.10
Average (isotopic)	Ni–O	1.98	3.87	0.09
	Ni–O	2.19	0.80	0.10
Average (isomorphic)	M–O	1.99	3.86	0.09
	M–O	2.18	0.66	0.10

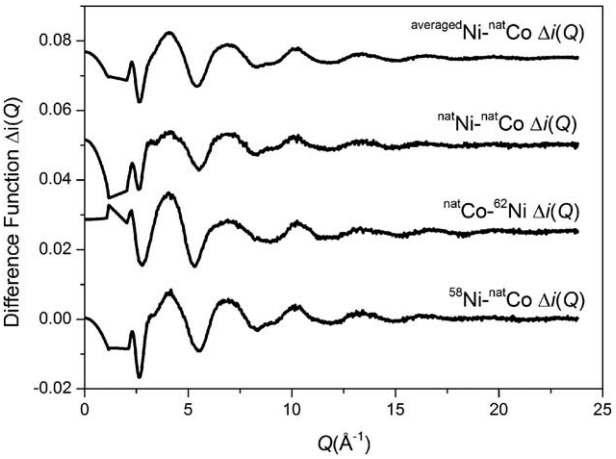

Fig. 5 First order difference isomorphic substitution functions $\Delta i(Q)$.

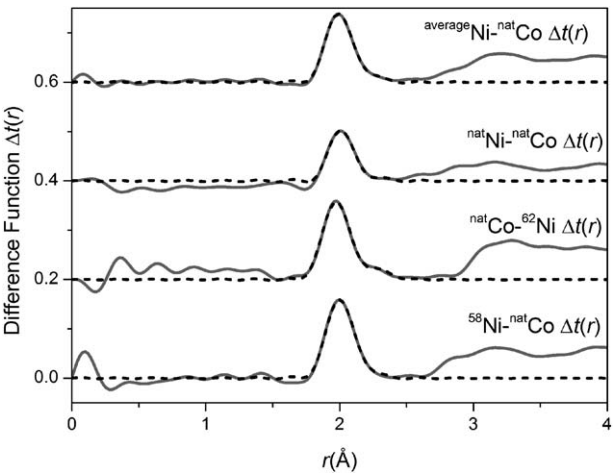

Fig. 6 Real space data for the isomorphic substitution difference functions. The solid curve represents the experimental data and the broken curve represents the resultant fits.

accordingly. The results do not preclude the possibility of a tiny fraction of Ni occupying a six fold. However, whilst octahedral Ni is common in crystalline materials it is rarely found in oxide silicate glasses.[44] Furthermore, 6-fold Ni–O typically exhibits a distinctive bright green colour which was not visible for the current glasses.[44] Galoisy and Calas have reported 5-fold Ni in a trigonal bipyramidal environment with minor amounts of four-fold Ni in $CaNiSi_2O_6$ glass.[42] In contrast they found predominantly 4-four Ni in glassy $K_2NiSi_3O_8$, whilst $Na_2NiSi_3O_8$ was found to have a mixture of 4- and 5-fold Ni.[43] They therefore concluded that the nickel environment is strongly dependent on the nature of alkali present. Brendebach *et al.* report that nickel occupies a predominantly octahedral environment in sodium phosphate systems with a Ni–O distance ~2.06 Å.[45] In the present system there is a relatively small fraction of phosphorus compared to silicon and Ni is found to adopt a predominantly 4- and 5-fold environment. This suggests that Ni does not show a particularly strong affinity for the phosphate species present within this glassy system.

Given that Ni has a similar charge: ion size ratio as Mg it would be reasonable to expect it to adopt a similar structural chemistry. However, the present data suggests that a minimum of 33% of Ni is 4-fold and therefore acting as a network former; this is significantly greater than the 14% Watts *et al.* reported for magnesium and suggests that there are important differences that were not predicted.[25] Bioglass doped with 3.8% NiO (or 1.37% metallic Ni) has a number density of 0.0769 atoms per Å^3 compared to 0.0757 atoms per Å^3 for 45S5 Bioglass. This represents a 1.6% increase in number density and also suggests that a proportion of Ni may act as a network former. Tetrahedral Ni will have shorter Ni–O bond lengths compared to higher coordinated Ni environments and would therefore be more likely to increase the number density.

Neutron diffraction with isomorphic substitution

Applying the method of isomorphic substitution[46,47] enables the local structural environment surrounding Co to be determined in a broadly analogous manner. The data allows three separate first order difference isomorphic substitution functions to be created ($\Delta i(Q)^{58Ni–Co}$, $\Delta i(Q)^{natNi–Co}$ and $\Delta i(Q)^{Co–62Ni}$) as shown in Fig. 5. The corresponding real-space, $\Delta T(r)$, functions are shown in Fig. 6. The difference in Ni/Co coherent scattering factors are 11.81, 7.81 and 10.89 for the $\Delta T(r)^{58Ni–Co}$, $\Delta T(r)^{natNi–Co}$ and $\Delta T(r)^{Co–62Ni}$ functions respectively. The optimum (weighted average) fit parameters for the isomorphic difference function are given in Table 1. As shown in Table 1, there is excellent agreement between the metal–oxygen, M–O, correlations obtained for Ni using the method of isotopic substitution and the Co/Ni datasets obtained using the method of isomorphic substitution. This confirms that Co and Ni are isostructural within these bioactive glasses.

The total diffraction patterns

The total diffraction patterns for the Ni and Co doped bioglasses were modelled using the NXFit program and the NDIS-derived fit parameters are given in Table 2. The results of a Ni/Co-free bioactive glass, prepared using an identical melt quench method, are also presented in Table 2 thus enabling a direct

Table 2 Structural parameters for the Ni and Co doped bioactive glasses obtained using the *NXFit* fitting routine. The parameters for 45S5 Bioglass *T*(*r*) are included for comparison.[22] Typical errors are ±0.02 Å on the peak position (r_{ij}), ±0.2 on the coordination number (N_{ij}) and ±0.02 Å on the disorder parameter (σ_{ij})

	^{58}Ni			^{nat}Ni			^{62}Ni			Co			Bioglass® 45S5		
	r (Å)	*N*	σ (Å)	*r* (Å)	*N*	σ (Å)	*r* (Å)	*N*	σ (Å)	*r* (Å)	*N*	σ (Å)	*r* (Å)	*N*	σ (Å)
P–O	1.57	4.0	0.02	1.57	4.0	0.01	1.58	4.0	0.03	1.57	4.0	0.03	1.60	4.0	0.01
Si–O	1.60	4.0	0.07	1.60	4.0	0.07	1.60	4.0	0.07	1.60	4.0	0.07	1.62	4.0	0.08
Ni–O	1.98	3.9	0.09	1.98	3.9	0.09	1.98	3.9	0.09	1.98	3.9	0.09	—	—	—
Ni–O	2.19	0.8	0.10	2.19	0.8	0.10	2.19	0.8	0.10	2.19	0.8	0.10	—	—	—
Na–O	2.34	3.1	0.14	2.33	3.1	0.13	2.32	3.1	0.13	2.32	3.1	0.13	2.33	3.1	0.15
Ca–O	2.30	5.3	0.11	2.31	5.3	0.12	2.32	5.3	0.12	2.31	5.3	0.12	2.35	5.3	0.11
Na–O	2.64	1.6	0.13	2.66	1.6	0.15	2.64	1.6	0.14	2.65	1.6	0.13	2.63	1.6	0.10
O–O	2.61	3.9	0.10	2.61	4.0	0.10	2.61	4.0	0.10	2.61	4.0	0.10	2.65	4.0	0.11
Ca–O	2.76	1.3	0.20	2.71	1.3	0.22	2.73	1.3	0.22	2.73	1.3	0.20	2.76	1.3	0.20

comparison of the present results with the archetypal 45S5 Bioglass®.[22] The 45S5 results were collected using the ISIS pulsed neutron source and full details of the data analysis are given by Martin *et al.*[22] To enable a direct comparison with the present data the reciprocal data was truncated at a Q_{max} of 23.7 Å (to match the present Ni (or Co) bioglass data) before Fourier transforming into real-space and fitting using the *NXFit* analysis program.

As expected, the short range order comprises ~4 oxygen atoms around Si at 1.6 Å[48] and ~4 oxygen around P at a separation between 1.5 and 1.6 Å.[49,50] The M–O correlations account for the region $2 < r$ (Å) < 2.2 as determined from the first order difference functions discussed above. The intermediate range order consists of overlapping Na–O, Ca–O, O–(P)–O and O–(Si)–O correlations and it is therefore not usually possible to resolve these unambiguously. Recently, by employing the method of isomorphic substitution, the Na–O[22] and Ca–O[23] correlations have been independently resolved in very similar glasses and a model has been proposed for the O–(X)–O correlation (where X = Si or P). These results provide an excellent starting point to begin modelling the overlapping correlations in the present data. The Ca–O feature was therefore modelled using two Ca–O distances based on recently obtained results for an analogous Ca/Sr bioglass system.[23] The values, determined for the Ni/Co bioactive glass system, of 5.3(1) oxygen atoms around Ca at 2.31(2) Å and 1.3(1) oxygen atoms around Ca at 2.73(3) Å are in good agreement with the previous reported values of 5.3 oxygen around Ca at 2.35 Å and 1.3 oxygen around Ca at 2.76 Å.[22] The Na–O feature was also modelled using two Na–O distances based on results recently obtained by the method of isomorphic substitution of a mixed Na/Li bioglass.[22] An asymmetric Na–O peak has been reported both experimentally in sodium silicates and in molecular dynamic simulations on sodium calcium silicates and on Bioglass®.[22,51,52] The Na–O values of 3.1 oxygen around Na at 2.33(1) Å and 1.6 oxygen around Na at ~2.65(2) Å obtained in this study are consistent with these results.[22] The first real space O···O correlation is expected to be dominated by O–(Si)–O correlations given that the concentration of Si is ~10 times greater than the concentration of P, and other O···O correlations such as O–(Ca)–O and O–(Na)–O are expected to occur at longer real space distances.[21] Given that Si is tetrahedrally coordinated, the expected O–(Si)–O distance is given by $\sqrt{8/3}r_{Si-O}$. The O–(Si)–O distance of 2.61 Å given in Table 1 is therefore in good agreement given the reported Si–O distance of ~1.6 Å. The O–(Si)–O coordination number also confirms that the network connectivity of the glass is largely unaffected by the addition of Ni or Co into these glasses, noting that *ortho*-silicates have an O–(Si)–O coordination number of 3 whilst a fully densified silica network would have an O–(Si)–O coordination number of 6.

Knowing the fraction of Ni (or Co) that acts as a network former enables the network connectivity of the glass to be calculated. If the network connectivity is too low, the glass dissolves too quickly and hydroxypatite does not have time to form – *i.e.* the bioactivity is effectively reduced. Conversely, if the network connectivity is too high, the glass does not release sufficient Ca and P for hydroxyapatite to form – reducing the bioactivity again. The network connectivity, NC, of a silicate glass is given by

$$NC = 4 - 2Z \quad (11)$$

with 4 representing a fully densified silica network and *Z* representing the number of excess oxygen per SiO_2. It therefore follows that the addition of NiO (or CoO) into a glass could either decrease the network connectivity (due to the additional oxygen incorporated) or increase the network connectivity if the metal (Ni or Co) adopts a network forming role. Assuming only 4-fold Ni (or Co) acts as a network formed then

$$Z = \frac{c_O - 4c_P}{c_{Si} + Rc_M} - 2 \quad (12)$$

where *R* is the fraction of the metal ions occupying a tetrahedral (network forming) environment. The phosphorus term takes into consideration its isolated orthophosphate environment where it binds to 4 oxygen atoms per phosphorus effectively removing these oxygen atoms from the network.

For the present system, given that 33% of Ni (or Co) occupies a network forming (tetrahedral) environment, it therefore follows that the network connectivity is 2.11 ± 0.02. This is very close to the connectivity required for optimal bioactivity and matches the network connectivity of Bioglass®. Hill recommends a network connectivity close to 2.0 for optimal bioactivity[53] whilst Watts *et al.* also note that all the very bioactive

glasses have a network connectivity close to 2.0.[25] Edén has shown that when the glass network becomes defragmented bioactivity decreases.[54] The time taken to form hydroxy-carbon apatite increased for glasses with connectivities of 2.01 and 1.97 compared to Bioglass (2.11). For the present system if the Ni (or Co) entered entirely as a network modifier the network connectivity would have fallen below these values, this suggests that the formation of 4-fold Ni (or Co) is important for maintaining optimal bioactivity. Currently, when designing Mg or Co glasses, multiple series are often manufactured based on the assumption that the metal ions act either entirely as network former or entirely as a network modifier.[25,27] Knowledge of the local environment of the Co and Ni ions will enable these systems to be better modeled. Furthermore, with this knowledge, and using the above network connectivity model, it is now possible to alter the network modifier concentration in a controlled fashion in order to compensate for the effects of Ni or Co and thus design bioactive glasses with optimal network connectivities. However, further work is still needed to determine the *in vitro* and *in vivo* properties of these materials.

4 Conclusions

Co and Ni doped bioactive glasses have been successfully manufactured. This is, to the best of our knowledge, the first time a bioactive glass containing Ni has been synthesised. Using the methods of isotopic and isomorphic substitution we have shown that Ni and Co adopt the same structural environment within these bioactive glasses. The cobalt and nickel-doped Bioglass samples reported here, represent one of the most complex amorphous materials (6 chemical elements and therefore 21 partial structure factors) and the lowest level of isomorphic enrichment (1.37 mol% Ni/Co) ever studied using isomorphic substitution for an amorphous system. The results confirm that Ni and Co act as network intermediates with a significant fraction adopting a four-fold symmetry, thereby entering the network. Importantly, there is no measureable difference in the remaining structure correlations (*e.g.* Si–O, P–O, Ca–O, Na–O and O–Si–O) between the archetypal 45S5 Bioglass® and these bioactive glasses doped with Ni or Co, indicating that the addition of these transition metals should not adversely affect the overall bioactivity or existing structural models. The data provided above will enable Ni and Co doped bioactive glasses to be rationally designed and optimised in the future according to network connectivity, dissolution and bioactivity requirements.

Acknowledgements

The authors wish to thank the Institut Laue-Langevin, ILL, for the allocation of beam-time. The work was part-funded by an EPSRC Project Studentship EP/F021011/1, and through the STFC's support of the ILL.

References

1 J. Malda, T. J. Klein and Z. Upton, *Tissue Eng.*, 2007, **13**, 2153.
2 D. Zou, Z. Zhang, J. He, K. Zhang, D. Ye, W. Han, J. Zhou, Y. Wang, Q. Li, X. Liu, X. Zhang, S. Wang, J. Hu, C. Zhu, W. Zhang, Y. Zhou, H. Fu, Y. Huang and X. Jiang, *Biomaterials*, 2012, **33**, 2097.
3 C. Wan, S. R. Gilbert, Y. Wang, X. Cao, X. Shen, G. Ramaswamy, K. A. Jacobsen, Z. S. Alaql, A. W. Eberhardt, L. C. Gerstenfeld, T. A. Einhorn, L. Deng and T. L. Clemens, *Proc. Natl. Acad. Sci. U. S. A.*, 2008, **105**, 686.
4 H. Abdollahi, L. J. Harris, P. Zhang, S. McIlhenny, V. Srinivas, T. Tulenko and P. J. DiMuzio, *J. Surg. Res.*, 2011, **165**, 112.
5 Q. Ke and M. Costa, *Mol. Pharmacol.*, 2006, **70**, 1469.
6 J. R. Jones, P. Sepulveda and L. L. Hench, *J. Biomed. Mater. Res.*, 2001, **58**, 720.
7 L. L. Hench, *J. Mater. Sci.: Mater. Med.*, 2006, **17**, 967.
8 V. FitzGerald, R. A. Martin, J. R. Jones, D. Qiu, K. M. Wetherall, R. M. Moss and R. J. Newport, *J. Biomed. Mater. Res., Part A*, 2009, **91**, 76.
9 R. A. Martin, H. Twyman, D. Qiu, J. C. Knowles and R. J. Newport, *J. Mater. Sci.: Mater. Med.*, 2009, **20**, 883.
10 R. A. Martin, S. Yue, J. V. Hanna, P. D. Lee, R. J. Newport, M. E. Smith and J. R. Jones, *Philos. Trans. R. Soc. London, Ser. A*, 2012, **370**, 1422.
11 I. D. Xynos, A. J. Edgar, L. D. K. Buttery, L. L. Hench and J. M. Polak, *Biochem. Biophys. Res. Commun.*, 2000, **276**, 461.
12 I. D. Xynos, A. J. Edgar, L. D. K. Buttery, L. L. Hench and J. M. Polak, *J. Biomed. Mater. Res.*, 2001, **55**, 151.
13 R. M. Moss, D. M. Pickup, I. Ahmed, J. C. Knowles, M. E. Smith and R. J. Newport, *Adv. Funct. Mater.*, 2008, **18**, 634.
14 S. P. Valappil, D. Ready, E. A. Abou Neel, D. M. Pickup, W. Chrzanowski, L. A. O'Dell, R. J. Newport, M. E. Smith, M. Wilson and J. C. Knowles, *Adv. Funct. Mater.*, 2008, **18**, 732.
15 A. Tilocca, *J. Mater. Chem.*, 2010, **20**, 6848.
16 A. Tilocca, A. N. Cormack and N. H. de Leeuw, *Chem. Mater.*, 2007, **19**, 95.
17 Y. Xiang and J. Du, *Chem. Mater.*, 2011, **23**, 2703.
18 A. Pedone, T. Charpentier, G. Malavasi and M. C. Menziani, *Chem. Mater.*, 2010, **22**, 5644.
19 A. Pedone, G. Malavasi and M. C. Menziani, *J. Phys. Chem. C*, 2009, **113**, 15723.
20 K. Fujikura, N. Karpukhina, T. Kasuga, D. S. Brauer, R. G. Hill and R. V. Law, *J. Mater. Chem.*, 2012, **22**, 7395.
21 V. FitzGerald, D. M. Pickup, D. Greenspan, G. Sarkar, J. J. Fitzgerald, K. M. Wetherall, R. M. Moss, J. R. Jones and R. J. Newport, *Adv. Funct. Mater.*, 2007, **17**, 3746.
22 R. A. Martin, H. L. Twyman, G. J. Rees, J. M. Smith, E. R. Barney, M. E. Smith, J. V. Hanna and R. J. Newport, *Phys. Chem. Chem. Phys.*, 2012, **14**, 12105.
23 R. A. Martin, H. L. Twyman, G. J. Rees, E. R. Barney, R. M. Moss, J. M. Smith, R. G. Hill, G. Cibin, T. Charpentier, M. E. Smith, J. V. Hanna and R. J. Newport, *J. Mater. Chem.*, 2012, **22**, 22212.
24 R. A. Martin, R. M. Moss, N. J. Lakhkar, J. Knowles, G. J. Cuello, M. E. Smith, J. V. Hanna and R. J. Newport, *Phys. Chem. Chem. Phys.*, 2012, **14**, 15807.

25 S. J. Watts, R. G. Hill, M. D. O'Donnell and R. V. Law, *J. Non-Cryst. Solids*, 2010, **356**, 517.
26 R. A. Martin, P. S. Salmon, D. L. Carroll, M. E. Smith and A. C. Hannon, *J. Phys.: Condens. Matter*, 2008, **20**, 115204.
27 M. M. Azevedo, G. Jell, M. D. O'Donnell, R. V. Law, R. G. Hill and M. M. Stevens, *J. Mater. Chem.*, 2010, **20**, 8854.
28 R. Shannon, *Acta Crystallogr., Sect. A: Cryst. Phys., Diffr., Theor. Gen. Crystallogr.*, 1976, **32**, 751.
29 A. Tilocca and A. N. Cormack, *J. Phys. Chem. B*, 2007, **111**, 14256.
30 Y. C. Fredholm, N. Karpukhina, D. S. Brauer, J. R. Jones, R. V. Law and R. G. Hill, *J. R. Soc. Interface*, 2012, **9**, 880.
31 I. Catelas, A. Petit, H. Vali, C. Fragiskatos, R. Meilleur, D. J. Zukor, J. Antoniou and O. L. Huk, *Biomaterials*, 2005, **26**, 2441.
32 C. Wu, Y. Zhou, W. Fan, P. Han, J. Chang, J. Yuen, M. Zhang and Y. Xiao, *Biomaterials*, 2012, **33**, 2076.
33 B. Ravel and M. Newville, *J. Synchrotron Radiat.*, 2005, **12**, 537.
34 A. Tenderholt, B. Hedman and K. O. Hodgson, PySpline: a modern, cross-platform program for the processing of raw averaged XAS edge and EXAFS data, in *X-ray absorption fine structure-XAFS13*, ed. B. Hedman and P. Painetta, 2007, vol. 882, p. 105.
35 S. J. Gurman, N. Binsted and I. Ross, *J. Phys. C: Solid State Phys.*, 1984, **17**, 143.
36 H. E. Fischer, P. Palleau and D. Feltin, *Phys. B*, 2000, **276**, 93.
37 M. A. Howe, R. L. McGreevy and P. Zetterstrom, *Computer Code CORRECT: Correction Program for Neutron Diffraction Data NFL Studsvik*, 1996.
38 G. J. Cuello, *J. Phys.: Condens. Matter*, 2008, **20**, 244109.
39 P. H. Gaskell, *Glasses and Amorphous Materials, Materials Science and Technology*, 9th edn, 1991, p. 175.
40 R. M. Moss, PhD thesis, University of Kent, 2009.
41 V. F. Sears, *Neutron News*, 1992, **3**, 26.
42 L. Galoisy and G. Calas, *Am. Mineral.*, 1991, **76**, 1777.
43 L. Galoisy and G. Calas, *Am. Mineral.*, 1992, **77**, 677.
44 L. Galoisy, *Elements*, 2006, **2**, 293.
45 B. Brendebach, R. Glaum, M. Funke, F. Reinauer, J. Hormes and H. Modrow, *Z. Naturforsch. A*, 2005, **60A**, 449.
46 R. A. Martin, P. S. Salmon, C. J. Benmore, H. E. Fischer and G. J. Cuello, *Phys. Rev. B: Condens. Matter Mater. Phys.*, 2003, **68**, 054203.
47 R. A. Martin, P. S. Salmon, H. E. Fischer and G. J. Cuello, *J. Non-Cryst. Solids*, 2004, **345–346**, 208.
48 B. E. Warren and J. Biscce, *J. Am. Ceram. Soc.*, 1938, **21**, 49.
49 R. A. Martin, P. S. Salmon, H. E. Fischer and G. J. Cuello, *J. Phys.: Condens. Matter*, 2003, **15**, 8235.
50 R. A. Martin, P. S. Salmon, H. E. Fischer and G. J. Cuello, *Phys. Rev. Lett.*, 2003, **90**, 185501.
51 A. N. Cormack and J. C. Du, *J. Non-Cryst. Solids*, 2001, **293**, 283.
52 A. Tilocca, *J. Chem. Phys.*, 2008, **129**, 084504.
53 R. Hill, *J. Mater. Sci. Lett.*, 1996, **15**, 1122.
54 M. Edén, *J. Non-Cryst. Solids*, 2011, **357**, 1595.